Research Article

Received: 11 May 2017 Revised: 30 July 2017 Accepted article published: 4 August 2017 Published online in Wiley Online Library: 30 September 2017

(wileyonlinelibrary.com) DOI 10.1002/jctb.5401

Iron(III)-modified tungstophosphoric acid supported on silica-pillared montmorillonite as catalysts for fructose conversion to methyl levulinate

Fengjiao Lai,[a,b*] Jia Luo,[a] Dan Jiang,[c] Tongchao Su[c] and Fan Zhang[a]

Abstract

BACKGROUND: Because of the decline in conventional sources of energy and the increasing pollution, the fossil fuel based energy structures is being replaced by renewable energy based structures such as biomass energy. Among current biodiesel sources, methyl levulinate (ML) obtained from catalytic conversion of renewable carbohydrate with methanol has received a great deal of attention. Silica-pillared montmorillonites (MMTSi) functionalized by iron-modified tungstophosphoric acid (HPWFe) were prepared, and their physicochemical properties and catalytic effects on ML production studied.

RESULTS: Catalysts characterization demonstrated the high dispersion and Keggin structure of HPWFe in the framework of MMTSi. Effects of various reaction parameters and catalyst recycling on the reaction performance were studied to optimize fructose conversion. With 4-HPWFe-MMTSi as the catalyst, an optimized ML yield of around 74 mol% was obtained at 180°C for 1 h, and the recovered catalyst after calcination was found to retain high activity after being reused five times.

CONCLUSION: The prepared HPWFe-MMTSi catalysts showed high porosity, perfect Brønsted-Lewis acidity and high thermal stability, which made their catalytic activity for fructose conversion and catalyst reusability values higher than others reported in the literature.

Supporting information may be found in the online version of this article.

Keywords: tungstophosphoric acid; iron; silica-pillared clay; fructose conversion; methyl levulinate

INTRODUCTION

Because of the increasingly serious problems of fossil energy depletion and environmental pollution, exploiting clean renewable energy resources has already become urgent.[1–3] Biomass energy, as one form of renewable energy with widely available resources, could not only help the energy crisis but also lower the environmental pollution.[2,3] Therefore, researching and developing chemical or biological transformations converting biomass into different biofuels and feedstock chemicals has become an important part of exploring new energy sources in the world.[4–6] Among these explorations of biomass energy, levulinate esters, owing to their unsaturated groups of carbonyls and esters, are versatile reaction intermediates and chemical feedstocks, and are widely used in the flavouring, fragrance, medical and plasticizer industries.[7–9] Moreover, when added to biodiesel as a blending component, levulinate esters improve lubrication, low temperature fluidity and flash point stability of biodiesel to lower the sulfur contents and finally realize cleaner-burning.[10]

In previous research, using an inorganic liquid acid (especially sulfuric acid) as catalyst was the most common method for levulinate esters production. Although the catalytic performance was good, the utilization of inorganic liquid acid has several problems such as separation difficulty, low recycling rate and persistent equipment corrosion.[11,12] In contrast, solid acid catalysts could avoid these problems and have aroused many researchers' interest. Nevertheless, only a limited number of solid acids such as SO_3H-functionalized materials, sulfated metal oxides, ion-exchange resin, and modified zeolites were available for producing levulinate esters from biomass.[13,14] Moreover, the yields of levulinate esters are still unsatisfactory. Owing to these problems, it is extremely important and necessary to develop efficient and environmentally benign catalysts for economical conversion of biomass feedstocks into levulinate esters.

Heteropoly acids (HPAs), owing to their strong acidity, especially those with the Keggin structure (such as $H_3PW_{12}O_{40,}$ HPW) have

* *Correspondence to: F Lai, Key Laboratory of Tropical Plant Resources and Sustainable Use, Xishuangbanna Tropical Botanical Garden, Chinese Academy of Sciences, Kunming 650223, China. E-mail: lfj0916@163.com*

a *Key Laboratory of Tropical Plant Resources and Sustainable Use, Chinese Academy of Sciences, Kunming, China*

b *University of Chinese Academy of Sciences, Beijing, China*

c *University of Science and Technology of China, Hefei, China*

shown excellent catalytic performance in both heterogeneous and homogeneous catalytic reactions.[15] HPW as a Brønsted acid has even higher acidity than H_2SO_4 but HPW utilization is limited due to its low surface area, poor thermal stability, and so on.[16] According to several reports, even if HPW was loaded in porous materials such as alumina, active carbon, titania, molecular sieve and ordered mesoporous silica, large HPW loss from the supports appeared in polar reaction media.[17–21] Since the diameter of Keggin heteropolyanion is about 1 nm,[21] encaging HPW into the high surface area frameworks with slightly larger size than the heteropolyanion might be a feasible method for improving the properties of HPW. Moreover, metal ion substituted HPW such as HPWFe or HPWTi contains both Brønsted and Lewis acid sites and shows better catalytic activity compared with pure HPW.[22,23] Therefore, metal-modified HPW supported on suitable porous materials might be an efficient solid acid catalyst for carbohydrates conversion to levulinate esters.

Montmorillonite (MMT) is a typical inorganic material and very rich clay mineral, and consists of layers of two tetrahedral silica sheets sandwiching one octahedral alumina sheet.[24–26] A series of ordered mesoporous clay materials based on montmorillonite known as silica pillared clay (MMTSi) materials have recently been prepared.[25,27] These inorganic porous materials have controllable pore dimensions and have specific catalytic properties depending on the type of silicate layers, pillaring agents and encapsulated functional molecules, and have stimulated a great deal of interest for potential application in a wide range of industries.[25] It is expected that the modified clay with textural mesoporosity could provide the opportunity for high dispersion of functional acid catalyst, as well as easy diffusion of reactants to active sites and products out of the pores.

In the present study, a sol–gel method and self-assembly method were applied to incorporate iron-modified HPW (HPWFe) into the framework of mesoporous MMTSi materials to synthesize a new solid acid catalyst. The resultant materials possess higher dispersion of the acid sites due to high surface area, and simultaneously overcome the low stability and leaching problem of HPWFe. The structure, appearance and other properties of the catalysts were analyzed using several characterization methods. The catalysts were applied in the conversation of carbohydrates to methyl levulinate (ML) to evaluate the catalytic activity. In addition, the influence of different process parameters including reaction temperature, reaction time, catalyst dosage and carbohydrate type on ML production was investigated. Meanwhile, the recyclability and stability of the catalysts were also studied for more practical applications.

Table 1. Results of XRF analysis of the samples

Catalyst sample	P_2O_5 (wt%)	WO_3 (wt%)	Fe (wt%)	HPWFe (wt%)	P:W:Fe
1-HPWFe-MMTSi	0.18	6.41	0.14	6.88	1:10.90:0.99
2-HPWFe-MMTSi	0.27	9.75	0.21	10.46	1:11.05:0.99
3-HPWFe-MMTSi	0.48	17.15	0.39	18.41	1:10.94:1.03
4-HPWFe-MMTSi	0.83	29.61	0.64	31.78	1:10.92:0.98
5-HPWFe-MMTSi	1.01	36.23	0.86	38.88	1:10.98:1.08

EXPERIMENTAL DETAILS

Materials

Cetyltrimethylammonium bromide (CTAB), concentrated hydrochloric acid (HCl, 36 wt%), tetraethyl orthosilicate (TEOS), $FeCl_3{\cdot}6H_2O$ (98%), D-fructose (99%), Amberlite FPA53 (Type 732), glucose (99%), starch, sucrose (98%), cellulose, ethanol (99.5%) and methanol (99.5%) were purchased from Aladdin Industrial Inc. Tungstophosphoric acid ($H_3PW_{12}O_{40}{\cdot}8H_2O$, HPW) and cellulose (microcrystalline, powder) were obtained from Sigma-Aldrich (Shanghai). Methyl levulinate (ML, 99%) was purchased from J&K Scientific Ltd (Beijing). All solvents and reactants are commercially available and were used without further purification. The natural

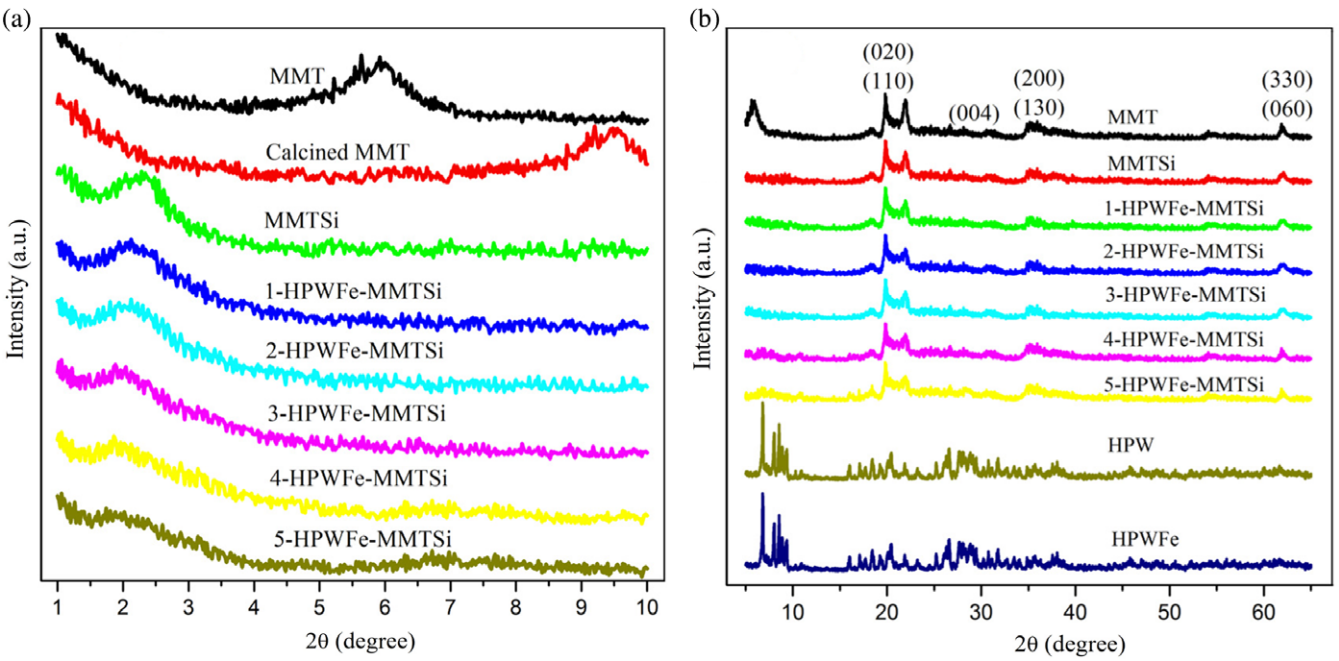

Figure 1. (a) Low-angle XRD patterns of samples; (b) wide-angle XRD patterns of samples.

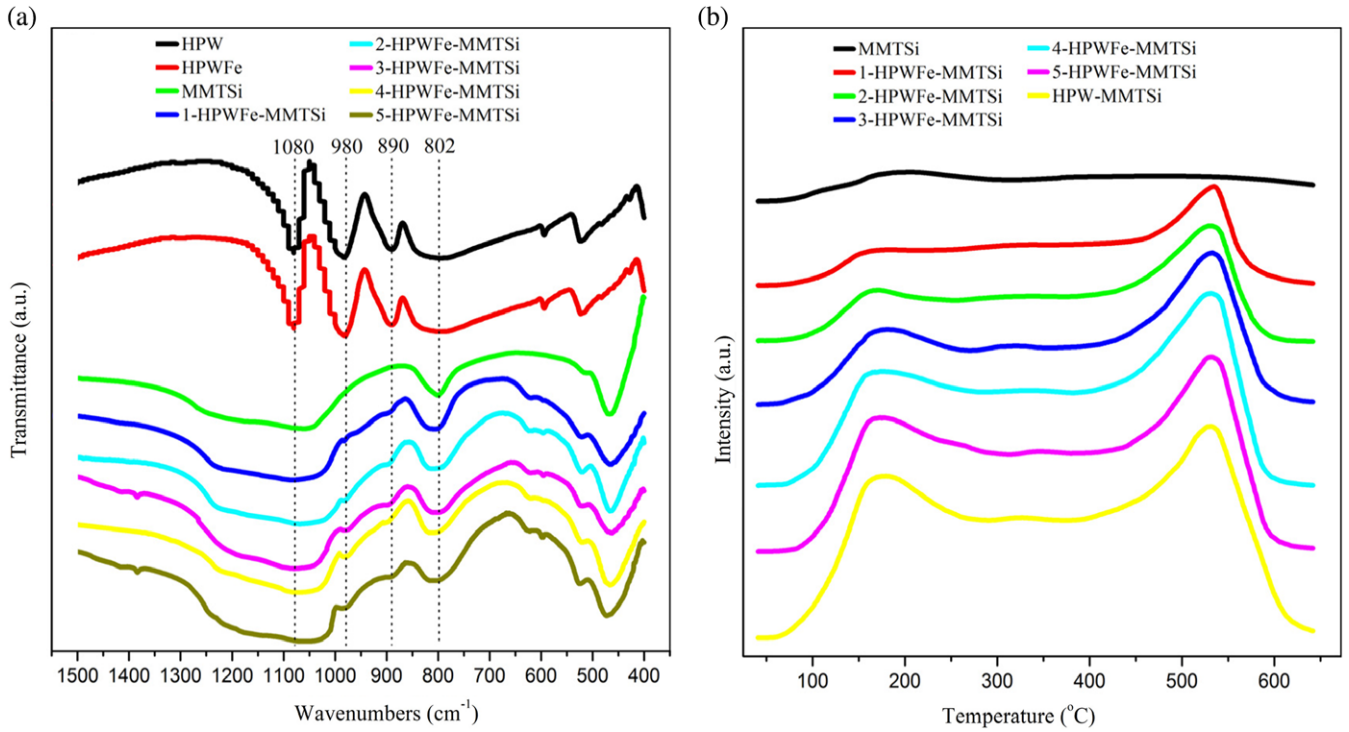

Figure 2. (a) FT-IR spectra of the samples; (b) NH_3-TPD curves of the samples.

montmorillonite clay (MMT) was obtained from the Zhejiang Yi-Guo Technological Reagent Co., Ltd (China), and used without any further purification or cations exchanging.

Catalysts preparation

HPWFe synthesis: first $Na_7PW_{11}O_{39}$ was prepared according to reference [28]. Subsequently, $Na_7PW_{11}O_{39}$ (5 mmol) and $FeCl_3{\cdot}6H_2O$ (5 mmol) were dissolved in 5 wt% H_2SO_4. The pH of the mixture was adjusted to 5.5 by $NaHCO_3$, followed by adding KCl (20 mmol) to form a precipitate. The precipitate was filtrated and recrystallized with water three times into potassium salt $K_4PW_{11}FeO_{39}$. Then 2 g of prepared $K_4PW_{11}FeO_{39}$ was dissolved in 1000 mL of deionized water, and strong-acid cation exchange resin (Amberlite FPA53, Type 732) was added to replace the potassium cations to obtain $H_4PW_{11}FeO_{39}$ (denoted as HPWFe). The final HPWFe powder was obtained by solvent evaporation at 50 °C and drying at 70 °C. The formation of HPWFe underwent the following reactions:[28]

$$\left[PW_{11}O_{39}\right]^{7-} + Fe^{3+} + 4K^{+} \rightarrow K_4PW_{11}FeO_{39} \quad (1)$$

$$K_4PW_{11}FeO_{39} + 4H^{+} \rightarrow H_4PW_{11}FeO_{39} \quad (2)$$

HPWFe supported on silica-pillared MMT (MMTSi): HPWFe and MMT composite catalysts were prepared by the combination of a sol–gel method and self-assembly method. A certain amount of MMT was added in 150 mL of deionized water and stirred for 1 h at room temperature to form a suspension solution. Then 12.5 mL of 28.6 wt% CTAB solution dissolved in ethanol was added dropwise into the suspension and stirred for 1 h, resulting in a gel mixture. The pH of the resultant gel was adjusted to 1.0 by dropwise addition of HCl aqueous solution. Subsequently, the requisite amount of HPWFe was dissolved in 10.0 mL of water and then added dropwise into the above mixture.

After stirring for 4 h, a white precipitate was obtained and then TEOS as silicon source was added, followed by continuous stirring for 12 h. The molar ratio of MMT, CTAB, TEOS, alcohol, water and HPWFe was 1:0.4:1.6:6.3:258:x. Then, the above precipitate was transferred to a PTFE-lined autoclave and aged for 24 h at 110°C in the mother liquor. Afterwards, the excess water was evaporated and the catalyst obtained was dried at 110°C and calcined at 400°C for 6 h in air. Finally, the HPWFe and MMT composite catalyst was obtained and labeled 1 to 5-HPWFe-MMTSi with different weight percentages of HPWFe in the prepared catalysts measured by X-ray fluorescence analysis (XRF). The sample without addition of HPWFe was also prepared following the same procedure and labeled MMTSi.

Catalyst characterization

Different elemental content in the samples was analyzed by X-ray fluorescence spectrometer (XRF, Philips Magix-601, Netherlands). The morphology of different samples was examined by scanning electron microscopy (SEM, ZEISS EVO LS10, Cambridge, UK). The crystalline structure was analyzed by X-ray diffraction (XRD, Rigaku Rotaflex RAD-C, Tokyo, Japan) equipped with a Cu Kα radiation source (40 kv and 200 mA) and 2θ data were collected from 2° to 90°. The characteristics of the molecular structure of the samples were analyzed by Fourier transform infrared spectroscopy (FTIR, Nicolet is10, Thermo Fisher Scientific, America) with a resolution of 4 cm^{-1} in the range 400–4000 cm^{-1}. Ammonia temperature programmed desorption (NH_3-TPD, Chemisorption analyzer, Quantachrome Instruments, Boynton Beach, FL, America) was also used to determine the acid density. Catalyst at around 0.2 g was treated under NH_3 flow (10% NH_3 and 90% He) for absorption at 50 °C for 1 h after degassing and then flushed with He for 1 h to remove the physically adsorbed NH_3. The NH_3-TPD data were recorded from 50°C to 650°C with a ramp of 10°C min^{-1}. The background curve was also obtained by treating catalyst under pure

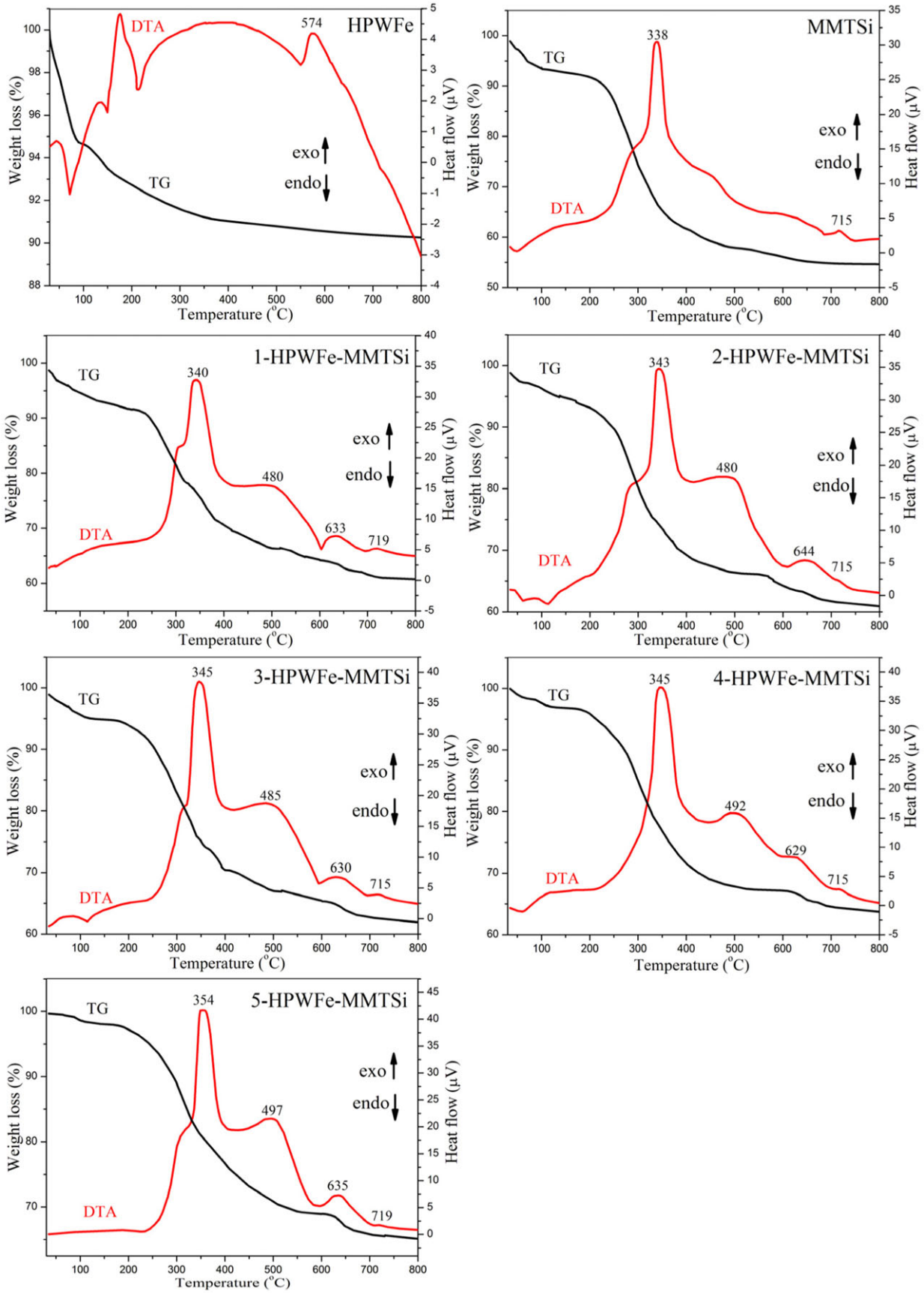

Figure 3. TG-DTA curves of the samples.

He instead of NH_3 flow during the adsorption step. Three different volumes (0.5, 1, 1.5 mL) of standard NH_3 gas (10% NH_3 and 90% He) were used to calibrate acidity. The final acidity of the catalyst needed to subtract the acidity of the background. The thermogravimetric and differential thermal analysis (TG-DTA, STA 449 C, NETZSCH, Germany) was applied to determine thermal effect of the samples in the range of 30–800°C in air. The surface area, pore size distribution and pore volume of catalysts were analyzed by Brunauer–Emmett–Teller method (BET, Tristar II 3020, Micromeritics Instruments, Atlanta, GA, America) with N_2 adsorption.

Reaction test and products analysis

The experiments were carried out in a 50 mL micro high-pressure autoclave (YZPR-50, Yanzheng Shanghai Experimental Instrument Co., Ltd). For each experiment, fructose (0.8 g), methanol (25 mL), and a given weight amount of solid acid catalyst were mixed to form a suspension and were poured into the autoclave. The autoclave was then heated to the desired temperature with magnetic stirring (500 rpm) and initial pressure (2 MPa N_2). After running the reaction for the desired duration, the autoclave was taken from the stove and quenched in an ice cool water bath to terminate the reaction. The liquid product and solid acid catalyst were separated by filtration.

Methyl levulinate (ML) and methyl formate in the reaction products were analyzed by gas chromatography (GC; GC-2014, Shimadzu, Kyoto) with a capillary column of Rtx-Wax (30 m × Ø0.25 mm × 0.25 μm) and a flame ionization detector. n-butyl alcohol was added in the liquid products as an internal standard, and the amount of ML in the reaction products was determined using calibration curves obtained by analyzing standard solutions with known amounts. Carbohydrate conversion was quantified by HPLC with RI detection (LC-20A, Shimadzu). The conversions from monosaccharides (fructose and glucose) and sucrose were calculated on a carbon-basis as the above equation for fructose. But the conversions from polysaccharide (starch and cellulose) also needed to subtract the concentration of unreacted biomass (namely solid residue) after reaction.

Carbohydrate conversions and ML yields were calculated using the following equations:

$$\text{Monosaccharide conversion } (\%) = \left[\left(C_0 - C_i\right)/C_0\right] \times 100 \quad (3)$$

$$\text{Polysaccharide conversion } (\%) = \left[\left(C_h - C_i - C_j\right)/C_h\right] \times 100 \quad (4)$$

$$\text{ML yield } (\text{mol}\%) = \left[\left(C_k \times M_0\right) / \left(C_0 \times M_k\right)\right] \times 100$$
$$\text{or } \left[\left(C_k \times M_h\right) / \left(C_h \times M_k\right)\right] \times 100 \quad (5)$$

where C_0 and C_i are the initial and post-reaction concentration of monosaccharide, respectively. C_0 and C_i are the initial and post-reaction concentration of polysaccharide calculated by monosaccharide, respectively. C_k is the concentration of ML produced by acid-catalyzed alcoholysis. The terms M_0, M_h and M_k represent the molecular weight of monosaccharide, the molecular weight of polysaccharide calculated by monosaccharide and ML, respectively. All the ML yields were gained from the average value of three parallel reactions.

RESULTS AND DISCUSSION

Catalyst characterization

The testing results of XRF for the prepared samples are shown in Table 1. These samples contained various HPWFe loadings (6.88, 10.46, 18.41, 31.78 and 38.88 wt%) but all showed the molar ratio of P:W:Fe ≈ 1:11:1, confirming the formation of mono-metal substituted undeca-tungstophosphates and the successful encapsulation of HPWFe into MMTSi.

To investigate the building of predesigned intercalated architecture in the samples, small-angle XRD was applied by analyzing the

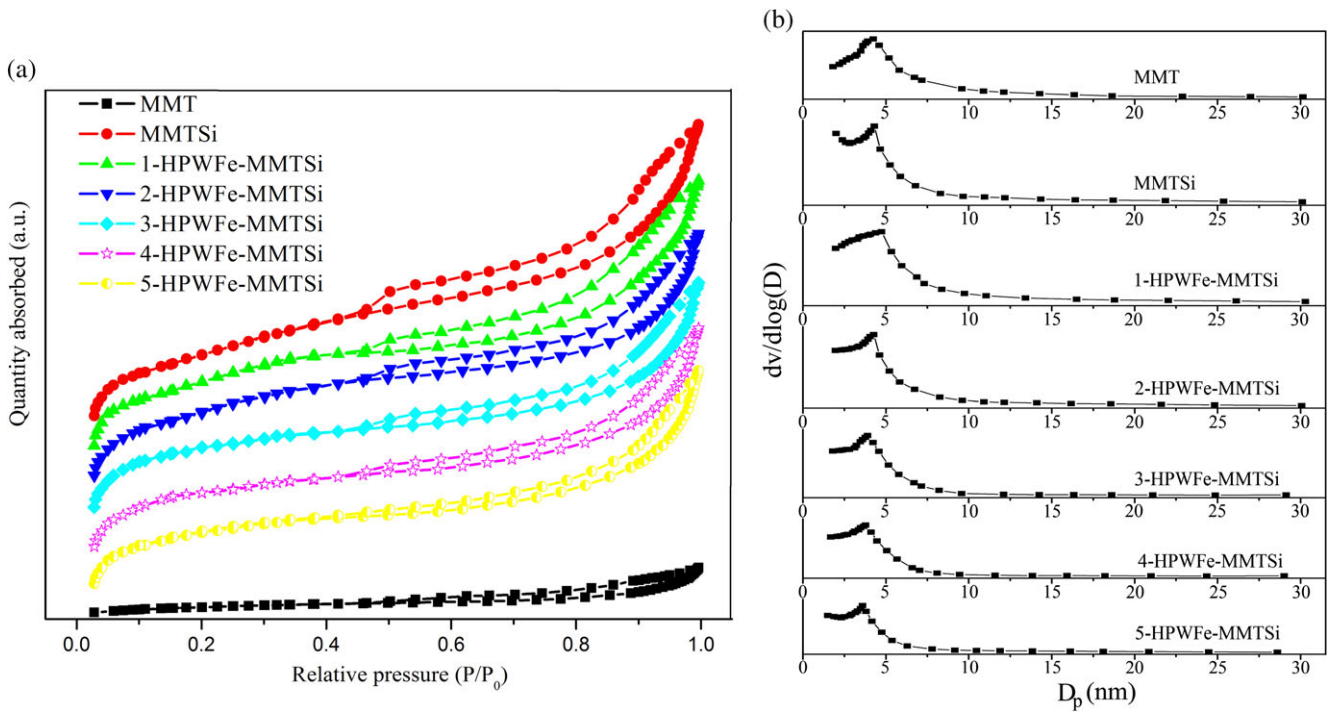

Figure 4. (a) N_2 adsorption/desorption isotherms of the samples; (b) pore size distribution curves of the samples.

Table 2. Textural properties of MMT, MMTSi, and different HPWFe-MMTSi samples

Sample	Average pore diameter (nm)	BET surface area ($m^2\ g^{-1}$)	Pore volume ($cm^3\ g^{-1}$)	Total acidity ($mmol\ g^{-1}$)
MMT	4.44	68	0.14	–
MMTSi	4.56	638	1.02	0.152
1-HPWFe-MMTSi	4.36	593	0.94	0.195
2-HPWFe-MMTSi	4.18	536	0.85	0.242
3-HPWFe-MMTSi	4.01	425	0.71	0.353
4-HPWFe-MMTSi	3.82	292	0.55	0.438
5-HPWFe-MMTSi	3.71	187	0.37	0.443
HPWFe-MMTSi	–	–	–	0.476

gallery distance. Thus small-angle XRD patterns of MMT, calcined MMT, MMTSi and different HPWFe-MMTSi samples are shown in Fig. 1(a). The diffraction peak (001) of MMT and calcined MMT were centered at $2\theta = 5.64°$ and $2\theta = 9.20°$, respectively. Therefore the interlayer spacing (d) for MMT and calcined MMT was 1.57 nm and 0.96 nm, respectively, calculated by the Bragg's equation:

$$2d\sin\theta = n\lambda \quad (6)$$

where d is the interlayer spacing, θ is the angle of incidence, λ is wavelength and n is an integer that denotes the order of the reflection.

According to related publications, the thickness of the clay sheet of MMT is around 0.96 nm.[25] Therefore, the lamellar structure of MMT has collapsed under calcination at 400°C. But for MMTSi, the diffraction peak (001) centered at $2\theta = 2.04°$ corresponds to the interlayer spacing (d) of 4.32 nm. Then the gallery distance of MMTSi was obtained as 3.36 nm by subtracting the thickness of clay sheet (0.96 nm) from the interlayer spacing (3.87 nm). These results suggested that with the addition of CTAB template and TEOS, stable mesoporous lamellar structure had been successfully formed during the MMTSi preparation process. For 1-HPWFe-MMTSi sample, diffraction peak (001) centered at around $2\theta = 1.98°$, corresponding with interlayer spacing of 4.46 nm and gallery distance of 3.50 nm. Moreover, with the increase of HPWFe content, the diffraction peak shifted to lower angles, corresponding to the enlarged interlayer spacing. Herein, it could be speculated that the encapsulation of HPWFe did not disturb the formation of intercalated structure of MMTSi. However, the diffraction intensity reduced gradually as the amount of HPWFe increased. This might be due to the poor dispersion or agglomeration of excessive HPWFe. Therefore, the amount of HPWFe loading has an appropriate value and should be obtained from further study.

The wide-angle XRD patterns of MMT, MMTSi and various HPWFe-MMTSi samples are presented in Fig. 1(b). The characteristic peaks of MMT at $2\theta \approx 19.8°, 26.8°, 35.1°$ and 61.9° were assigned to (110), (020), (004), (130), (200), (330), and (060) diffractions.[25] In addition, these characteristic peaks could also be observed in MMTSi, and all HPWFe-MMTSi samples. This suggested that the addition of TEOS and HPWFe did not destroy the laminated crystalline structure of MMT. HPW showed characteristic peaks related to Keggin ion at $2\theta = 10.28°, 18.44°, 20.46°, 23.22°, 26.28°, 30.76°, 35.72°$ and 38.06°,[20] which could also be observed in HPWFe. This confirmed the presence of Keggin structure in HPWFe catalyst. But these characteristic peaks related to the Keggin ion could hardly be seen in the 1-HPWFe-MMTSi to 4-HPWFe-MMTSi samples, but could in 5-HPWFe-MMTSi, indicating that HPWFe could be highly dispersed in the lamellar structure of MMTSi when the loading was around or below 30 wt%.

The FT-IR spectra of pure HPW, HPWFe, MMTSi and different HPWFe-MMTSi samples in the region 400–1600 cm^{-1} are shown in Fig. 2(a). Pure HPW showed several infrared absorption peaks at around 1080, 980, and 890 cm^{-1}, representing ν_{as}(P-O), ν_{as}(W=O), and ν_{as}(W-O_b-W) in corner shared octahedral,[18] respectively. And these characteristic bands of HPW were preserved in the spectrum of HPWFe, suggesting that HPWFe kept the Keggin structure of HPW. However, in the spectra of HPWFe-MMTSi samples with low HPWFe content, the peaks at 980 and 890 cm^{-1} were significantly covered by the peaks of MMTSi. When the HPWFe content was more than that in 3-HPWFe-MMTSi, the infrared absorption peaks of HPWFe could be clearly observed. Moreover, with the increase of HPWFe content, the intensity of these peaks was evidently strengthened and shifted to a higher wavenumber region. In the spectra of HPWFe, the broad band around 802 cm^{-1} could be attributed to ν_{as} (W-O_c-W) in the edge shared octahedral.[18] In the spectrum of MMTSi, the band at 795 cm^{-1} was assigned to the symmetric stretching frequency of Si-O-Si.[29] But for HPWFe-MMTSi, an infrared absorption band was observed at around 815 cm^{-1}. This might be ascribed to the formation of Si-O-W bonds between MMTSi and HPWFe, demonstrating that HPWFe had been well encaged into the structural framework of MMTSi.[29] These results indicated that the Keggin structure of HPWFe was successfully supported on MMTSi, as did the results of wide-angle XRD.

NH_3-TPD was carried out to measure the strength and density of acid sites in MMT, MMTSi, HPW-MMTSi (contains the same HPW content as 4-HPWFe-MMTSi without iron) and different HPWFe-MMTSi samples (Fig. 2(b)). According to Hidalgo theory, a desorption peak at over 350°C corresponds with a strong acid site; a contrary peak is related to a weak acid site. It was observed that MMTSi possessed two desorption bands at around 200 °C and 470 °C, corresponding to weak acid site and medium strong acid site, respectively. The total acid amount of MMTSi was only 0.152 mmol g^{-1}. For sample encapsulating HPWFe, namely, HPWFe-MMTSi samples, the strong acid center shifted to around 520°C and weak acid center barely changed. At the same time, the strong acid intensity and the total acid amount was significantly enhanced, resulting from the fact that HPW is a strong acid and has a strong acid center at around 550°C.[16] The reason that the strong acid center of HPW decreased to around 520°C might be attributed to the interaction between partial protons of HPW and Si-OH of MMTSi, which could obviously improve the stability of catalysts but also make some strong acid sites change to weak acid sites. In addition, the desorption band at around 520°C was evidently intensified with increasing HPWFe content up to 4-HPWFe-MMTSi, while 5-HPWFe-MMTSi showed a markedly reduced intensity. It was proposed that the deposition of excessive HPWFe in 5-HPWFe-MMTSi might lead to blockage of the pore channels, thus hindering the acid sites inside from exposure to the NH_3.[17] Therefore, the acid amount of HPWFe-MMTSi increased with the increase of HPWFe content first and reached 0.438 mmol g^{-1} for 4-HPWFe-MMTSi, but 5-HPWFe-MMTSi (0.443 mmol g^{-1}) showed a comparable acid amount to 4-HPWFe-MMTSi. Moreover, the total acid amount of 4-HPWFe-MMTSi (0.438 mmol g^{-1}) was smaller than that of HPW-MMTSi (0.476 mmol g^{-1}), but its ML yield from fructose was lower than that of 4-HPWFe-MMTSi under the

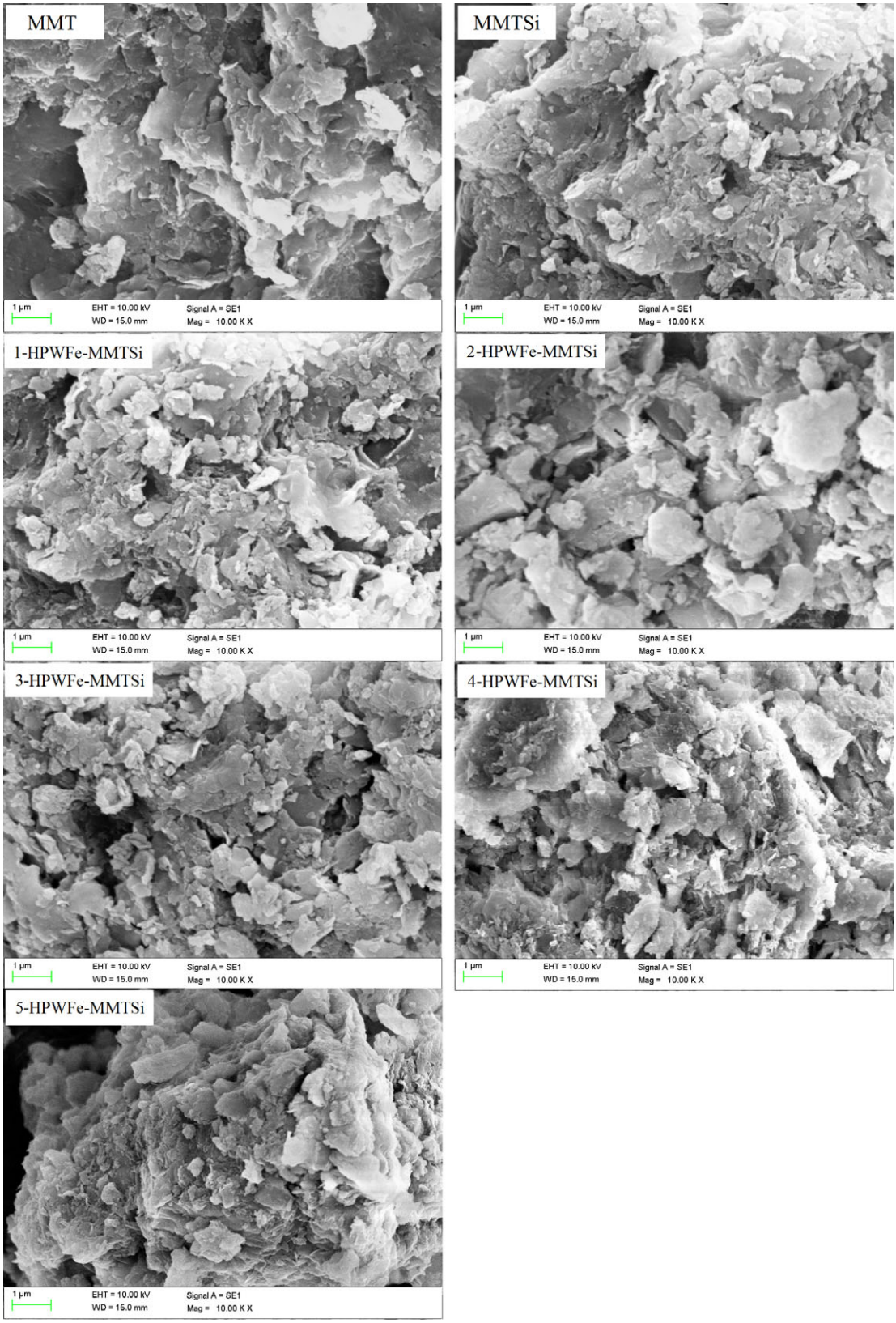

Figure 5. SEM images of the samples.

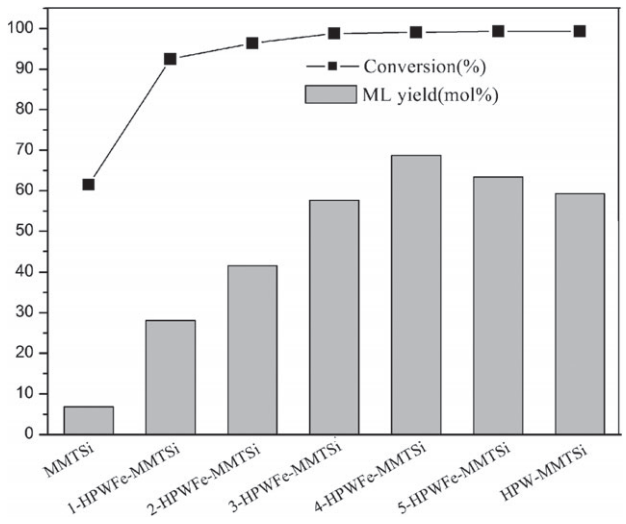

Figure 6. Conversion of fructose to methyl levulinate using various catalysts (0.8 g fructose, 0.35 g catalyst and 25 mL methanol at 180°C for 1 h).

same reaction conditions. This was because that mono-substituted HPW performed the downward trend for Brønsted acidity[23] but the introduced Lewis acid sites could promote the alcoholysis of fructose to ML (as the proposed reaction pathway in Fig. S1, Supporting material).[30]

The TG-DTA curves of the HPWFe, MMTSi, and HPW-MMTSi sample in the region 30–800°C are shown in Fig. 3. For all the samples, the weight loss observed before 100°C was attributed to the loss of physically absorbed water molecules and the corresponding DTA curve in this region was endothermic.[31,32] For HPWFe, the weight loss (about 4.18%) between 100 and 296°C was assigned to the loss of crystal water of the Keggin unit, corresponding to the endothermic peak centered at 211°C in the DTA curve.[29] The final step of about 3.88% weight loss in the range of 296–570°C was assigned to the loss of acidic protons and the beginning of decomposition of the Keggin structure, corresponding to the endothermic peak centered at about 400°C in the DTA curve.[29,32] And the endothermic peak centered at 572°C was attributed to the collapse of the heteropoly acid structure to form corresponding oxides.[29,32] For MMTSi sample, there was a sharp exothermic peak in the range 210–400°C centered at 333°C, accounting for the decomposition of CTAB. This result indicated that CTAB template could be eliminated through calcination at 400°C.[33] And the last exothermic peak centered at around 715°C in the DTA curve was ascribed to the collapse of the mesoporous gallery structure.[34] For HPWFe-MMTSi samples, the endothermic peak corresponding to the loss of HPW acidic protons shifted to around 480°C, indicating that HPW could be generated and well encaged in the framework of MMTSi. Moreover, the endothermic peak accounting for the complete decomposition of the heteropoly acid also shifted to around 630°C in the DTA diagrams of HPW-MMTSi. These results suggested that the thermal stability of HPWFe in the HPWFe-MMTSi samples was much higher than that of merely HPWFe. Moreover, the decomposition temperature of CTAB increased to around 340°C, which might be ascribed to the interation of CTAB and HPW to some extent. The exothermic peak corresponding to the collapse of the structure of the silica-pillared MMT could also be observed in all the DTA curves HPWFe-MMTSi samples, suggesting that the interlayer gallery structure of MMTSi was maintained after loading HPWFe. These were in accordance with the results of XRD and FT-IR.

The hysteresis loops of isotherms and the pore-size distributions of MMT, MMTSi and all the HPWFe-MMTSi samples are shown in Fig. 4 and the textural properties such as surface area, average pore size, and pore volume are presented in Table 2. MMTSi and all the HPWFe-MMTSi samples showed type IV isotherm patterns with H4-type hysteresis loop starting at about 0.45 partial pressure (Fig. 4(a)), confirming their mesoporous structures with the cylindrical pores formed in the gallery region.[35] The MMT sample presented an isotherm with adsorption at low relative pressure ($P/P0 < 0.3$) and a small hysteresis loop at high relative pressures ($P/P0 = 0.50–0.95$), corresponding to small amount of mesopores (Type IV).[35] The hysteresis loops of the isotherm of HPWFe-MMTSi samples were obviously much larger than that of MMT, but lower than that of the MMTSi sample. Moreover, the hysteresis loop of the isotherm decreased as the HPWFe content increased. Figure S2 illustrates the proposed formation mechanism of the ordered mesoporous MMTSi and HPWFe-MMTSi materials.[29] As expected, MMTSi showed a high surface area of 638 $m^2 g^{-1}$, which was much higher than that of natural MMT (68 $m^2 g^{-1}$), indicating that the mesoporous silica-pillared MMT was well formed by the addition of TEOS. For HPWFe-MMTSi samples, the surface area and pore volume were also much larger than that of MMT, but lower than that of MMTSi. And as the HPWFe loading was increased, surface area, pore diameter (Fig. 4(b)) and pore volume all strongly decreased. The reason being, as the HPWFe loading increased on MMTSi, HPWFe species entered the pores of MMTSi and then decreased the average pore diameter, and the average pore volume as well as the surface area.[20] Moreover, the HPWFe loaded in the HPWFe-MMTSi samples contributed to the sample weight which could also affect the surface area.

The morphologies of the samples are shown in Fig. 5. It can be seen that MMTSi kept the lamellar structure of nature MMT but swelled a little.[25] HPWFe-MMTSi also exhibited lamellar structure and was similar to the morphology of MMTSi, indicating that the introduction of HPWFe did not destroy the interlayer gallery structure of MMTSi.

Catalytic performance

Effect of different catalysts

Preliminary experiments were carried out to evaluate the catalytic performance of MMTSi and different HPWFe-MMTSi catalysts for ML production from fructose at 180°C for 1 h (Fig. 6). Among the solid catalysts tested, only 61.5% fructose conversion and 6.8 mol% ML yield were obtained from MMTSi catalyst. For 1-HPWFe-MMTSi samples, fructose conversion and ML yield increased significantly to above 90% and 28.1 mol%. Combined with the results of NH_3-TPD test in Fig. 2(b), the strong acid intensity of 1-HPWFe-MMTSi was significantly elevated compared with that of MMTSi. Therefore, the acid strength of catalysts is a key factor for the formation of ML and the strong acid sites of HPWFe could improve ML yield. For 1-HPWFe-MMTSi to 4-HPWFe-MMTSi with gradually increasing HPWFe content, ML yield increased from 28.1 to 68.7 mol% due to the increasing acidity, indicating that the acidity of catalysts is crucial for the formation of ML. But ML yield for 5-HPWFe-MMTSi was 63.4 mol% which was lower than that of 4-HPWFe-MMTSi. This could be attributed to the agglomeration of excessive HPWFe molecules in the interlayer regions of 5-HPWFe-MMTSi catalyst, which could prevent reactant molecules reaching acid sites in catalysts and then decrease reaction activity. This phenomenon was consistent with the N_2 adsorption–desorption test results.

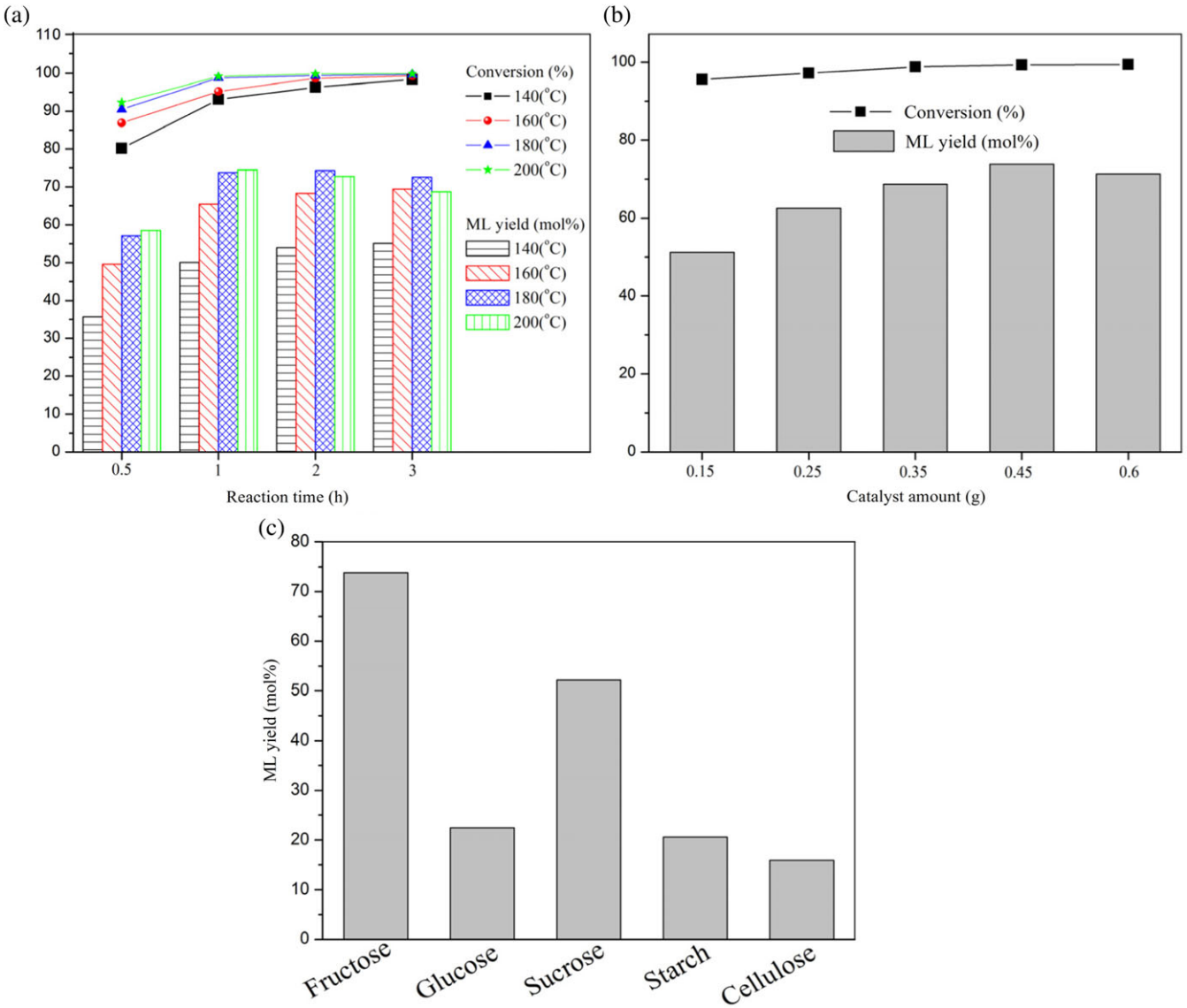

Figure 7. (a) Effect of reaction time and temperature (0.8 g fructose, 0.45 g catalyst and 25 mL methanol); (b) effect of catalyst dosage (0.8 g fructose and 25 mL methanol at 180°C for 1 h); (c) conversion of various carbohydrates (0.8 g substrate, 0.45 g 4-HPWFe-MMTSi catalyst and 25 mL methanol at 180 °C for 1 h, but at 220 °C for 5 h when the substrate is cellulose).

Table 3. Comparison of different catalysts for the production of ML from fructose

Catalyst	Temperature (°C)	Time (h)	ML yield (mol%)	Ref.
sulfated montmorillonite	200	4	65	24
Sulfated TiO_2-ZrO_2	200	1	71	8
Amberlyst 15	170	15	68	4
Nafion NR50	170	15	73	4
PD-En-SO_3H	170	15	78	4
4-HPWFe-MMTSi	180	1	74	This work

To investigate the effect of iron element in HPWFe, catalytic activity of 4-HPWFe-MMTSi was compared with HPWFe-MMTSi (contains the same HPW content as 4-HPWFe-MMTSi without iron). The results showed that ML yield through 4-HPWFe-MMTSi was higher than that from HPW-MMTSi, indicating that the iron substituted HPW supported on MMTSi was more active compared with parent HPW supported on MMTSi. This might be due to the generation of Lewis acid sites (Fe^{3+} ions), which was in line with previous research that the combination of Brønsted acid with Lewis acid could effectively promote the alcoholysis of fructose to levulinate esters.[16] Combining the physiochemical properties of the catalysts with catalytic results, it could be deduced that the number of accessible active acid sites, the acid types and the accessibility of the organic reactants to the active sites markedly effected the overall activity resulting from the relationship of catalyst properties and catalytic results. Above all, 4-HPWFe-MMTSi was chosen as the most appropriate catalyst for further experiments.

Effect of reaction time and temperature

4-HPWFe-MMTSi was applied for the study of the influence of reaction time and temperature on ML yield (Fig. 7(a)). At a relatively low temperature of 140 °C, around 80% fructose was converted after 0.5 h with ML yield of only 35.7 mol%. As reaction time

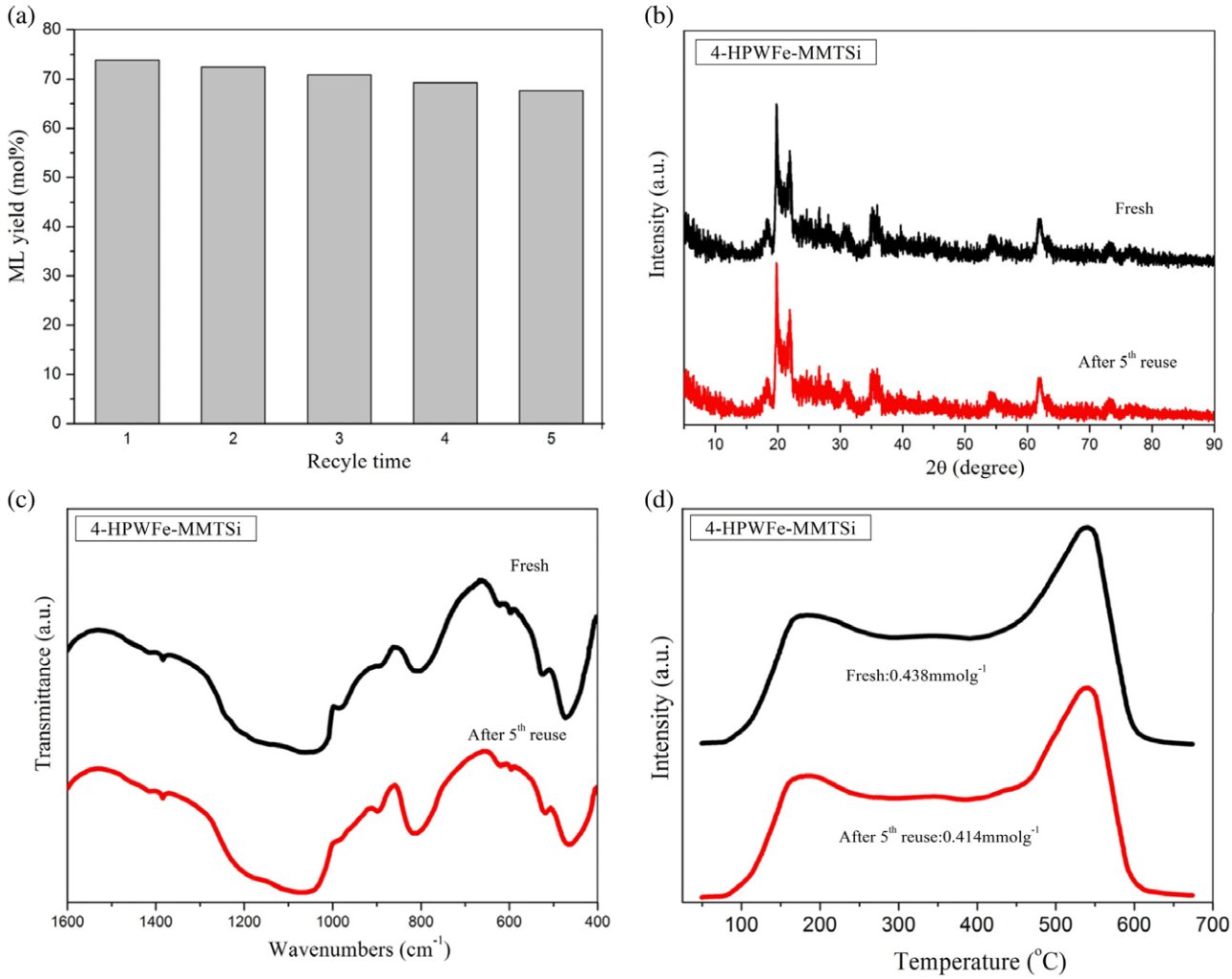

Figure 8. Recyclability of 4-HPWFe-MMTSi catalyst for fructose conversion (0.8 g fructose, 0.45 g catalyst and 25 mL methanol at 180 °C for 1 h) (a) conversion and ML yield vs number of cycles as well as (b) XRD patterns, (c) FT-IR spectra, and (d) NH_3-TPD profiles for fresh and recycled (after 5 cycles) 4-HPWFe-MMTSi catalysts.

rose to 3 h, fructose conversion increased to above 98% and ML yield grew to the maximum value of 55.1 mol%. The moderate ML yield lower than expected resulted from the stable intermediates unable to proceed to downstream reactions according to previous research.[13] At a higher temperature of 160 °C, a higher ML yield of 65.4 mol% with 95.2% fructose conversion was observed within just 1 h. And ML yield gradually rose from 65.7 to 69.4 mol% with almost complete conversion when time was increased from 1 to 3 h. These results demonstrated that both temperature and time played an important role in the further transformation of intermediates into the final product ML. At a much higher temperature of 180 °C, ML yield increased from 57.1 to 73.8 mol% at a time from 0.5 to 1 h and then remained nearly at a constant level, indicating that the reactants had reached near-equilibrium conversion. At 200°C, ML yield reached the maximum value of 74.5 mol%, which was comparable with ML yield at 180°C after 1 h. With further increase of reaction time, it was found that the reaction solution gradually turned brown and ML yield decreased to 68.7 mol% after 3 h. This might be due to the fact that side-reactions occur at excessively high temperature, bringing about numerous polymers and humins.[13] In addition, ML could be decomposed to other substances at high temperature.[13] Therefore, the temperature of 180 °C along with 1 h reaction time was selected as the optimal condition for further experiments.

Effect of catalyst dosage

Catalyst dosage determines the availability of the acidic sites, and its influence on ML production from fructose was evaluated by using 4-HPWFe-MMTSi as catalyst (Fig. 7(b)). It was found that with increasing catalyst dosage from 0.15 to 0.45 g, fructose conversion increased from 95% to nearly 100% and ML yield increased from 51.26 to 73.8 mol%. These could be explained by low catalyst dosage containing low acid density and not reaching reaction equilibrium in 1 h. With the increase of catalyst loading, the increased total number of acid sites led to a faster reaction rate to promote fructose conversion and a higher ML yield in a given time. But for catalyst dosage of 0.6 g, ML yield decreased to 71.3 mol%. It could be deduced that a proper catalyst dosage with enough active sites produced good catalytic effect on the reaction and ML yield reached maximum, but excessive catalyst only contributed to additional side-reactions. Taking the cost and efficiency into consideration, 0.45 g catalyst was chosen as an optimal amount in subsequent experiments.

Conversion of various carbohydrates

To explore the scope of application of HPWFe-MMTSi for ML production from other reaction substrates, fructose, sucrose, starch and cellulose were employed in alcoholysis reactions using 4-HPWFe-MMTSi catalyst under the same reaction conditions except for cellulose. As shown in Fig. 7(c), a much lower ML yield of 22.5 mol% was obtained from glucose. The distinction of catalytic effect on both hexoses might be ascribed to the higher stabilization of the ring structure of glucose, and the reaction pathway from glucose also contains isomerisation to fructose to form ML.[30] The disaccharide sucrose, consisting of one glucose and one fructose unit,[30] gave a medium amount of ML (52.2 mol%), between those from fructose and glucose. When starch was used as substrate, 20.6 mol% ML yield was obtained, which was close to that from glucose. This might be due to the solubility state of starch at high temperature,[13] which facilitated the conversion of starch to methyl glucoside intermediate to form ML. The ML yield from cellulose (15.9 mol%) was significantly lower than that from glucose even when improving temperature to 220°C and prolonging the time to 5 h. Since cellulose consists solely of 1-4-β-linked anhydro-D-glucose, the hydrogen bonding and Van der Waals forces in the cellulose molecules is relatively more difficult to break down than other carbohydrates.[24] In addition, the insolubility of cellulose in near-critical methanol also contributes to the difficulty of cellulose conversion.[13]

Research on fructose conversion to ML was compared with other reported heterogeneous acids under respective optimized reaction conditions (Table 3). It is observed that 65 mol% and 71 mol% of ML yield were obtained by sulfated montmorillonite and sulfated TiO_2-ZrO_2, respectively, but a high temperature of 200°C was required and their catalytic activity was found to be greatly reduced after each run.[8,24] For Amberlyst 15, Nafion NR50 and PD-En-SO_3H, a very long reaction time (15 h) was necessary to achieve high ML yield (68–78 mol%) from fructose.[4] In this work, 4-HPWFe-MMTSi catalyst remarkably improved the reactions in terms of reaction temperature (down to 180 °C) and reaction time (down to 1 h) with a comparable ML yield (around 74 mol%).

Catalyst recycling

For future industrial application, the long-term stability and reusability of HPWFe-MMTSi catalyst was investigated by reusing 4-HPWFe-MMTSi for ML production under the same reaction conditions. After each recycling, the recovered catalyst was washed with ethanol three times and dried at 110 °C overnight before it was reused in a new experiment. The results (Fig. 8(a)) showed that the catalytic activity had no significant decrease after five runs. Combining the previous results of XRD (Fig. 1), FT-IR (Fig. 2(a)) and SEM (Fig. 5) analysis, the excellent reusability of 4-HPWFe-MMTSi catalyst was because the HPWFe had been well encaged in the silica-pillared framework of MMTSi, resulting in high stability and negligible loss of HPWFe after each run. Moreover, the XRD pattern (Fig. 8(b)) and FT-IR spectrum (Fig. 8(c)) of the recovered 4-HPWFe-MMTSi were well consistent with those of the fresh material, proving that the silica-pillared and Keggin structured 4-HPWFe-MMTSi catalyst remained intact in recycles. Thus, 4-HPWFe-MMTSi could easily restore catalytic activity. Based on the NH_3-TPD measurement (Fig. 8(d)), it was obvious that the acid sites (0.414 mmol g^{-1}) of catalyst reused five times also showed no dramatic changes in comparison with acid sites of fresh 4-HPWFe-MMTSi catalyst (0.438 mmol g^{-1}). In conclusion, 4-HPWFe-MMTSi catalyst was stable and active for high yield ML production.

CONCLUSIONS

In this research, a series of mesoporous HPWFe-MMTSi catalysts with HPWFe content of 6.88–38.88 wt% were successfully prepared by sol–gel synthesis and the self-assembly method. Catalysts characterization confirmed that HPWFe was highly dispersed in the framework of mesoporous silica-pillared MMT, and also retained the Keggin structure. 4-HPWFe-MMTSi catalysts showed excellent catalytic activity for glucose conversion to ML with balanced content of MMT, Fe and HPW and reached around 74 mol% ML yield at 180°C for 1 h. In addition, after being recycled five times, 4-HPWFe-MMTSi catalyst retained its structure and high acidity, leading to only a small decrease in ML yield. Therefore, the prepared HPWFe-MMTSi samples can be considered as potential solid acid catalysts for the production of levulinate esters from cellulosic biomass and deserve further studies.

ACKNOWLEDGEMENT

The authors wish to acknowledge financial support from the Youth Innovation Promotion Association CAS (No. 2017440), the Natural Science Foundation of Yunnan Province of China (No. 2015FB184, No. 2017FB015), and the Natural Science Foundation of China (No. 31400518, No. 31400507). We also thank Professor Zhen Fang (Department of Engineering, Nanjing Agricultural University) and Professor Jianghua Chen (Key Laboratory of Tropical Plant Resources and Sustainable Use, Xishuangbanna Tropical Botanical Garden, Chinese Academy of Sciences) for their kind assistance and advice on this study.

Supporting Information

Supporting information may be found in the online version of this article.

REFERENCES

1 Sanders JPM, Clark JH, Harmsen GJ, Heeres HJ, Heijnen JJ, Kersten SRA *et al.*, Process intensification in the future production of base chemicals from biomass. *Chem Eng Process* **51**:117–136 (2012).
2 Climent MJ, Corma A and Iborra S, Conversion of biomass platform molecules into fuel additives and liquid hydrocarbon fuels. *Green Chem* **16**:516–547 (2014).
3 Baliban RC, Elia JA and Floudas CA, Biomass to liquid transportation fuels (BTL) systems: process synthesis and global optimization framework. *Energy Environ Sci* **6**:267–287 (2013).
4 Pan H, Liu X, Zhang H, Yang K, Huang S and Yang S, Multi-SO3H functionalized mesoporous polymeric acid catalyst for biodiesel production and fructose-to-biodiesel additive conversion. *Renew Energy* **107**:245–252 (2017).
5 Sheldon RA, Green and sustainable manufacture of chemicals from biomass: state of the art. *Green Chem* **16**:950–963 (2014).
6 Gallezot P, Conversion of biomass to selected chemical products. *Chem Soc Rev* **41**:1538–1558 (2012).
7 Démolis A, Essayem N and Rataboul F, Synthesis and applications of alkyl levulinates. *ACS Sustain Chem Eng* **2**:1338–1352 (2014).
8 Njagi EC, Genuino HC, Kuo CH, Dharmarathna S, Gudz A and Suib SL, High-yield selective conversion of carbohydrates to methyl levulinate using mesoporous sulfated titania-based catalysts. *Micropor Mesopor Mater* **202**:68–72 (2015).
9 Lomba L, Giner B, Bandrés I, Lafuente C and Pino MR, Physicochemical properties of green solvents derived from biomass. *Green Chem* **13**:2062–2070 (2011).
10 Joshi H, Moser BR, Toler J, Smith WF and Walker T, Ethyl levulinate: a potential bio-based diluent for biodiesel which improves cold flow properties. *Biomass Bioenergy* **35**:3262–3266 (2011).
11 Lange JP, Graaf van de WD and Haan RJ, Conversion of furfuryl alcohol into ethyl levulinate using solid acid catalysts. *Chem Sus Chem* **2**:437–441 (2009).

12 Mascal M and Nikitin EB, Comment on processes for the direct conversion of cellulose or cellulosic biomass into levulinate esters. *ChemSusChem* **3**:1349–1351 (2010).
13 Peng L, Lin L, Li H and Yang Q, Conversion of carbohydrates biomass into levulinate esters using heterogeneous catalysts. *Appl Energy* **88**:4590–4596 (2011).
14 Holm MS, Saravanamurugan S and Taarning E, Conversion of sugars to lactic acid derivatives using heterogeneous zeotype catalysts. *Science* **328**:602–605 (2010).
15 Shimizu K-I, Niimi K and Satsuma A, Polyvalent-metal salts of heteropolyacid as efficient heterogeneous catalysts for Friedel-Crafts acylation of arenes with carboxylic acids. *Catal Commun* **9**:980–983 (2008).
16 Gomes FNDC, Mendes FMT and Souza MMVM, Synthesis of 5-hydroxymethylfurfural from fructose catalyzed by phosphotungstic acid. *Catal Today* **279**:296–304 (2017).
17 Romanelli G, Vázquez P, Pizzio L, Quaranta N, Autino J, Blanco M *et al.*, Phenol tetrahydropyranylation catalyzed by silica-alumina supported heteropolyacids with Keggin structure. *Appl Catal A: Gen* **261**:163–170 (2004).
18 Sheng X, Kong J, Zhou Y, Zhang Y, Zhang Z and Zhou S, Direct synthesis, characterization and catalytic application of SBA-15 mesoporous silica with heteropolyacid incorporated into their framework. *Micropor Mesopor Mater* **187**:7–13 (2014).
19 Shen L, Feng Y, Yin H, Wang A, Yu L, Jiang T *et al.*, Gas phase dehydration of glycerol catalyzed by rutile TiO_2-supported heteropolyacids. *J Ind Eng Chem* **17**:484–492 (2011).
20 Kumar CR, Rambabu N, Maheria KC, Dalai AK and Lingaiah N, Iron exchanged tungstophosphoric acid supported on activated carbon derived from pinecone biomass: evaluation of catalysts efficiency for liquid phase benzylation of anisole with benzyl alcohol. *Appl Catal A: Gen* **485**:74–83 (2014).
21 Mukai SR, Lin L, Masuda T and Hashimoto K, Key factors for the encapsulation of Keggin-type heteropoly acids in the supercages of Y-type zeolite. *Chem Eng Sci* **56**:799–804 (2001).
22 Shimizu K-I, Furukawa H, Kobayashi N, Itaya Y and Satsuma A, Effects of Brønsted and Lewis acidities on activity and selectivity of heteropolyacid-based catalysts for hydrolysis of cellobiose and cellulose. *Green Chem* **11**:1627–1632 (2009).
23 Tao M, Xue L, Sun Z, Wang S, Wang X and Shi J, Tailoring the synergistic Bronsted-Lewis acidic effects in heteropolyacid catalysts: applied in esterification and transesterification reactions. *Scientific Reports* **5**:13764–13773 (2015).
24 Xu X, Zhang X, Zou W, Yue H, Tian G and Feng S, Conversion of carbohydrates to methyl levulinate catalyzed by sulfated montmorillonite. *Catal Commun* **62**:67–70 (2015).
25 Mao H, Zhu K, Li B, Yao C and Kong Y, Synthesis of titania modified silica-pillared clay (SPC) with highly ordered interlayered mesoporous structure for removing toxic metalion Cr(VI) from aqueous state. *Appl Surf Sci* **292**:1009–1019 (2014).
26 Chmielarz L, Piwowarska Z, Kuśtrowski P, Gil B, Adamski A, Dudek B *et al.*, Porous clay heterostructures (PCHs) intercalated with silica-titania pillars and modified with transition metals as catalysts for the DeNOx process. *Appl Catal B: Environ* **91**:449–459 (2009).
27 Yang S, Liang G, Gu A and Mao H, Synthesis of mesoporous iron-incorporated silica-pillared clay and catalytic performance for phenol hydroxylation. *Appl Surf Sci* **285P**:721–726 (2013).
28 Brevard C, Schimpf R, Tourne G and Tourne CM, Tungsten-183 NMR: a complete and unequivocal assignment of the tungsten-tungsten connectivities in heteropolytungstates via two-dimensional183 NMR techniques. *J Am Chem Soc* **105**:7059–7063 (1983).
29 Li B, Liu Z, Han C, Ma W and Zhao S, *In situ* synthesis, characterization, and catalytic performance of tungstophosphoric acid encapsulated into the framework of mesoporous silica pillared clay. *J Colloid Interf Sci* **377**:334–341 (2012).
30 Saravanamurugan S, Buu ONV and Riisager A, Conversion of mono- and disaccharides to ethyl levulinate and ethyl pyranoside with sulfonic acid-functionalized ionic liquids. *Chem Sus Chem* **4**:723–726 (2011).
31 Mueller R, Kammler HK, Wegner K and Pratsinis SE, OH surface density of SiO_2 and TiO_2 by thermogravimetric analysis. *Langmuir* **19**:160–165 (2003).
32 Ajaikumar S and Pandurangan A, HPW and supported HPW catalyzed condensation of aromatic aldehydes with aniline: synthesis of DATPM derivatives. *J Mol Catal A: Chem* **286**:21–30 (2008).
33 Kleitz F, Schmidt W and Schüth F, Calcination behavior of different surfactant-templated mesostructured silica materials. *Micropor Mesopor Mater* **65**:1–29 (2003).
34 Occelli ML, Catalytic cracking with an interlayered clay, a two dimensional molecular-sieve. *Ind Eng Chem Prod Res Dev* **22**:553–559 (1983).
35 Rojas F, Kornhauser I and Felipe C, Capillary condensation in heterogeneous mesoporous networks consisting of variable connectivity and pore-size correlation. *Phys Chem Chem Phy* **4**:2346–2355 (2002).